

Robot Navigation in Irregular Environments with Local Elevation Estimation using Deep Reinforcement Learning

Kasun Weerakoon, Adarsh Jagan Sathyamoorthy, Utsav Patel, and Dinesh Manocha

Abstract—We present a novel method for safely navigating a robot in unknown and uneven outdoor terrains. Our approach trains a novel Deep Reinforcement Learning (DRL)-based network with channel and spatial attention modules using a novel reward function to compute an attention map of the environment. The attention map identifies regions in the environment’s elevation map with high elevation gradients where the robot could have reduced stability or even flip over. We transform this attention map into a 2D navigation cost-map, which encodes the planarity (level of flatness) of the terrain. Using the cost-map, we formulate a novel method for computing local least-cost waypoints leading to the robot’s goal and integrate our approach with DWA-RL, a state-of-the-art navigation method. Our approach guarantees safe, locally least-cost paths and dynamically feasible robot velocities in highly uneven terrains. Our hybrid approach also leads to a low sim-to-real gap, which arises while training DRL networks. We observe an improvement of X% in terms of success rate, the cumulative elevation gradient of the robot’s trajectory, and the safety of the robot’s velocity. We evaluate our method on a real Husky robot in highly uneven real-world terrains and demonstrate its benefits.

I. INTRODUCTION

Autonomous wheeled robots have increasingly been used for numerous real-world field applications. For instance, they are used for indoor and outdoor surveillance in defense, search and rescue, planetary/space exploration, surveying large agricultural fields, etc. Each of these applications requires the robot to operate in a certain kind of terrain. Each of these terrains can be characterized by a set of properties such as texture, hardness or softness, unevenness, slope, etc. To effectively perform tasks while navigating on a certain terrain, robots must sense and understand its properties and make safe and stable navigation decisions.

The fundamental terrain properties that challenge wheeled mobile robots are the terrain’s unevenness and slope, i.e., the fine elevation changes at different locations in the robot’s immediate surroundings. Such fine elevation changes can significantly affect the quality of the robot’s trajectory, the torque required by the robot’s wheels (and in turn its energy consumption), its pose, and the probability of flipping over (or the robot’s stability).

In recent years, there have been numerous works in perception [1][2], control [3], and planning [4][5] that have tackled the problem of navigating in uneven outdoor terrains. In perception, semantic segmentation approaches for assessing a terrain’s navigability, and navigation, Deep Reinforcement Learning (DRL)-based [6][7] methods have demonstrated excellent results in terms of success rate and cumulative travel distance in certain outdoor environments.

However, these methods have a few key limitations. Semantic segmentation approaches classify pixels in an image into several pre-defined classes such as traversable, partially traversable, non-traversable, obstacle, background,



Fig. 1: Our robot navigating in an uneven terrain in a locally least-cost, safe trajectory. Our approach uses the environment’s elevation maps, computes an attention mask to identify decreased-stability regions on the maps, and computes a navigation cost-map. It then selects waypoints that can be reached by locally least-cost paths and integrates with DWA-RL [8] to navigate on the trajectory. Our approach guarantees that the paths are the safest locally and that the robot’s velocities are dynamically feasible.

etc. However, such discreet classifications are dependent on human annotations, which could lead to bias and the misclassification of traversable surfaces as non-traversable. Robot navigation methods that use such methods for perception plan highly conservative, sub-optimal trajectories. DRL-based navigation approaches, which are trained in simulations, are not limited by human annotations but possess a high sim-to-real transfer gap. That is, the performance of the DRL network trained in simulations degrades when transferred to real-world environments. Such methods also cannot provide any optimality guarantees on the robot’s trajectories. Moreover, the aforementioned methods are computationally intense (requiring desktop-grade CPU, GPU, and memory) for real-time performance, which makes many of them unsuitable for robots with limited processing capabilities.

Main contributions: We present a novel method for navigating a robot safely and stably in unknown, uneven terrains. Our approach computes an attention mask from an intermediate feature vector of a novel DRL network. The attention mask highlights locations that can decrease the robot’s stability (high elevation gradient or high risk of the robot flipping over). We refer to these locations as *decreased stability locations*. We combine the attention mask on the environment’s elevation map and transform it into a 2D navigation cost-map. We integrate it with DWA-RL [8], a state-of-the-art navigation method to guide our robot by computing least-cost waypoints. This hybrid formulation decouples sensing (to our network) and acting (to DWA-RL) and significantly reduces our overall approach’s sim-to-real gap. Our formulation is computationally light and

guarantees that the robot will navigate in locally least-cost trajectories (in the most planar regions) with dynamically feasible velocities. The novel components of our approach include:

- A fully trained end-to-end DRL network that computes robot velocities using normalized elevation maps of the environment, the robot’s pose, and the robot’s goal location as inputs. The network uses a Convolutional Block Attention Module (CBAM) [9] and a novel reward function that includes negative rewards (penalties) for velocities that result in unsafe robot orientations or the robot heading in directions with high elevation gradient. From an intermediate feature vector in the DRL network, we extract a spatial attention mask that accurately identifies decreased-stability regions in the environment. Our approach leads to an attention map that is not biased by human annotations.
- A 2D navigation cost-map computed using the extracted attention mask and a normalized elevation map of the environment. Each cost in the cost-map corresponds to a certain location and encodes the location’s planarity, which affects the robot’s stability. Using the cost-map leads to X% higher success rate.
- A method to compute waypoints that can be reached by locally least-cost trajectories for the robot to navigate to its goal. We use these trajectories as inputs to DWA-RL [8], a navigation method that computes dynamically feasible robot velocities. The waypoints are computed such that the robot navigates in regions with the least cumulative elevation gradients. This results in a decrease in the Trajectory Gradient Cost (TGC) of Y% and an improvement in the safety of the robot’s velocities by Z%. The hybrid combination with DWA-RL significantly reduces the sim-to-real gap of our overall approach.

II. RELATED WORK

In this section, we discuss existing work on the terrain understanding problem and robot navigation on uneven terrains.

A. Terrain Understanding Problem

The earliest works utilized classification and modeling techniques to address the terrain identification problem [10][11]. Model-based methods such as [12] estimate optimal navigable regions based on Gaussian process mixture models. In [13], laser range finders were used to estimate the roughness of the traversable regions. A Markov random field-based terrain model was proposed in [14] to refine noisy sensory inputs from LiDAR, stereo cameras, and infrared cameras to exploit terrain data inherent in agricultural outdoor environments.

Due to the increasing availability of complex deep neural network (DNN) models, recent methods have extended learning-based classification techniques towards terrain navigability estimation [15][16][17]. For example, [2] uses robot-ground interaction data to train DNNs to perform terrain classification tasks. The paper argues that deep CNNs can achieve comparable or better classification performance when contrasted with standard Support Vector Machine (SVM) approaches. Even though the classification

approaches can be trained or modeled to identify terrain features such as roughness, discontinuity, and navigability, such methods are insufficient to understand the diverse terrain and vegetation types found in real outdoor environments.

Most of features extracted from onboard sensors are heavily environment dependent. For example, visual features and external geometric features can vary significantly from one environment to another. Hence, elevation estimation methods were introduced to generalize the terrain understanding problem. In [18], a probabilistic occupancy estimation framework called “OctoMap” was introduced. A robot-centric elevation mapping approach based on range measurements was presented in [19]. Later, this concept was extended in [20] to obtain elevation maps based on proprioceptive localization from kinematic and inertial measurements. Recent studies such as [21] highlight the importance of terrain elevation data to perform robust outdoor navigation tasks.

B. Robot Navigation on Uneven Terrains

Initially, robot navigation on uneven terrains was treated as a binary classification problem by categorizing uneven terrain as obstacles or free space to navigate [22]. Later, methods such as [23] extended to continuous obstacle space by performing a deterministic search in spatially discretized state spaces. By expanding the previous concepts, a potential field-based navigation strategy was introduced in [24] to navigate unmanned ground vehicles (UGV) on rough terrains at higher speeds. The potential field was generated in a two-dimensional trajectory space of the UGV by considering dynamic constraints, terrain conditions, and navigation conditions.

Recent developments in deep learning models have allowed researchers to design motion planners with better learning capabilities [5][25]. For example, several methods such as [26][4] have incorporated on-board sensory inputs and prior knowledge of the environment to estimate cost functions or cost maps for robot navigation. In [27], a nonlinear geometric cost function has been trained to imitate the behavior of a human expert in uneven terrains. Similarly, an energy-cost model was proposed in [7] to generate energy-efficient paths on rough terrains for mobile robots.

Numerous navigation methods based on end-to-end DRL have been proposed to address the problem of uneven terrain navigation [21]. For example, [28] has utilized an elevation map, the robot’s orientation, and depth images to train an A3C model-based DRL framework. Similar work in [29] presented a Navigation Multimodal Fusion Network (NMFNet)-based learning strategy that depends on three visual input modalities: laser, RGB images, and point cloud data. In [30], the effectiveness of zero to local-range sensing was compared using a rainbow DRL-based local planner. The paper argues that robot-centric local range sensing provides better action outputs from the policy network than zero-range and immediate-range sensing inputs. All the aforementioned DRL methods were trained and tested only on simulated uneven terrains. Hence, transferring such methods into a real robot while maintaining comparable navigation performance will be challenging [6].

III. BACKGROUND

We discuss the background components used in our approach and define the notations used.

Symbols	Definitions
$E(i, j)$	An $n \times n$ 2-D elevation map of the sensed environment
c	Ground clearance of the robot
$E_N(i, j)$	Local 2-D elevation map normalized based on ground clearance
$A(i, j)$	Attention mask obtained from an intermediate feature vector
$C(i, j)$	Navigation cost-map
res	Resolution to convert index locations to real-world locations
r_{sense}	Radius (in meters) of the robot's sensing region
e_{max}, e_{min}	Max and min elevation values in $E(x, y)$ (in meters)
d_{goal}	Distance between the robot and its goal
α_{goal}	Angle between the robot's heading direction and the direction to the goal
$\alpha_{relative}$	Angle between the robot's current location and the goal w.r.t. the robot's start location
\mathbf{g}	Goal location relative to the robot
ϕ, θ	Roll and pitch angles of the robot

TABLE I: List of symbols used in our approach and their definitions.

A. Notations, Definitions, and Assumptions

We highlight the symbols and notation we use in Table I. Our formulation uses square elevation maps (from processed point cloud data) obtained from a 3D lidar with a range of r_{sense} . The lidar has a 360° field of view and is rigidly mounted on a four-wheeled differential drive robot. We assume that the robot's start and goal locations are in stable planar regions. For certain robot orientations, the lidar may not detect portions of the terrain since the lidar's rays could go to infinity. We assume that the undetected portions constitute less than 30% of the sensed environment.

All 2D data in our work (E, E_N, A, C) are regarded as $n \times n$ matrices or grids with the robot located at the center. We transform the indices to access the elements in these data such that the robot's position corresponds to $(0, 0)^{th}$ element. We obtain real-world positions (x, y) from indices (i, j) as

$$(x, y) = res * (i, j). \quad (1)$$

B. Deep Reinforcement Learning

We train an end-to-end DRL network based on the Deep Deterministic Policy Gradient (DDPG) algorithm [31] combined with Convolutional Neural Network layers and CBAM [9] (see Section III-C). We choose DDPG because it uses an actor-critic network, which leads to efficient learning compared to the individual performance from a policy-based or value-based learning method. We briefly describe the input and action spaces of our DRL network here and our novel network architecture and reward function in Section IV. The perception input consists of a 2D robot-specific elevation map ($E_N(i, j)$). The robot pose and goal related inputs include d_{goal} , α_{goal} , $\alpha_{relative}$, $|\phi|$, $|\theta|$ and the elevation gradient vector \mathbf{h} in the robot's heading direction defined as follows:

$$\begin{aligned} G &= \|\nabla E(i, j)\|_2 \\ \mathbf{h} &= G(n/2 : 1, 0). \end{aligned} \quad (2)$$

Where, ∇ denotes the gradient operation resulting in an $n \times n$ G matrix and $G(n/2 : 1, 0)$ denotes all the values in rows $n/2$ to 1 in the 0^{th} column (according to our

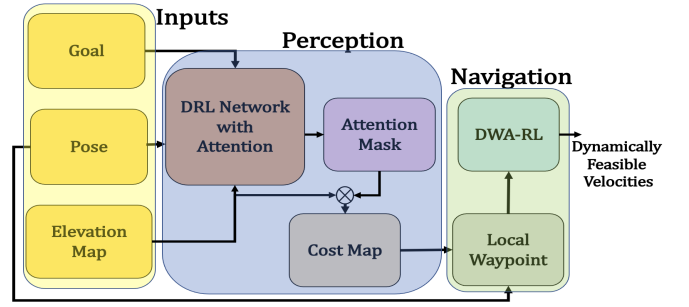


Fig. 2: Our overall system architecture. Our architecture decouples perception and navigation to different modules instead of using an end-to-end DRL network. This drastically improves the sim-to-real transfer capabilities of our method.

indexing conventions). The action space is a linear and angular velocity pair for the robot.

Although DRL methods are useful for training certain robot behaviors, they are highly data inefficient (require much higher quantities of input data and longer training episodes) and suffer from the sim-to-real gap (see Section I). In addition, the actions/velocities computed by the DRL network cannot guarantee that they will be dynamically feasible or optimal (in terms of any metric). Therefore, we choose not to use the output velocities from the DRL network. Instead, we extract an attention mask from an intermediate feature vector in the network (see Section IV-B.1 and Fig. 3), which we use to compute a cost-map, and least-cost max-velocity waypoints. Our formulation guarantees that the robot will navigate the safest local path and avoid flipping over.

C. Convolutional Block Attention Module

For an outdoor robot to successfully reach its goal, it needs to be aware of the regions where its stability could be adversely affected and avoid them. To focus on such relevant regions in the environment's elevation map, we use CBAM, a light-weight attention module that can be integrated with any CNN architecture [9]. Given a feature vector (say an output of a CNN) with a certain number of channels, CBAM sequentially applies attention modules along the channels and then along the spatial axis (different parts on the feature vector) to obtain a refined feature vector. Using CBAM with existing CNN architectures has led to significant accuracy and precision improvements in image classification applications, implying that the networks have learned exactly what features on which to focus.

IV. PROPOSED METHOD

In this section, we explain in detail three important components of our method: 1. the pre-processing stage of obtaining a normalized elevation map, 2. computing a navigation cost-map based on the attention mask from a novel DRL network, and 3. computing least-cost waypoints for the robot and integrating with DWA-RL.

A. Normalized Elevation Map

We use existing software packages to process raw point-cloud data from a 3D lidar and obtain an $n \times n$ local elevation map $E(i, j)$ around the robot. We employ nearest neighbor

interpolation to interpolate values for missing points based on nearby points.

A robot with higher ground clearance c can navigate through higher degrees of unevenness than a robot with lower ground clearance. We account for a robot's ground clearance by normalizing the local elevation map $E(i, j)$ by subtracting c from all of its elements and compute the normalized local elevation map $E_N(i, j)$ as,

$$E_N(i, j) = \begin{cases} (E(i, j) - c) + 0.1(e_{max} - e_{min}) & \text{if } E(i, j) - c > 0, \\ (E(i, j) - c) & \text{Otherwise.} \end{cases} \quad (3)$$

B. Computing Attention Mask

To compute the navigation cost-map, we first obtain an attention mask for the normalized local elevation map by training a DRL network. We explain our novel network architecture and the reward function used for training it in the following sections.

1) *Network Architecture*: Our novel network architecture is shown in Fig. 3. The network has two branches. On the first branch, to process the input normalized elevation map (with $n = 40$), we use a 2D convolutional layer of dimensions $40 \times 40 \times 8$. This outputs a feature vector with eight channels, which are passed on to the channel attention and spatial attention modules sequentially, and then the channels are passed through another convolutional layer. The channel and spatial attention modules weigh the features in the different channels and locations in each channel that identify decreased stability locations relevant for safe robot navigation. The resultant intermediate output is a refined feature vector (F_{ref}) with dimensions $40 \times 40 \times 8$, which is finally passed through a dimension reduction convolutional layer.

On the second branch, we concatenate the other inputs (d_{goal} , α_{goal} , $\alpha_{relative}$ $|\phi|$, $|\theta|$, and \mathbf{h} vector) to obtain a 1D vector of size $n/2 + 5$ (25 in this case). This is processed using a fully connected layer of dimensions shown in Fig. 3. The outputs from the two branches are concatenated through several fully connected layers to finally obtain the robot's linear and angular velocities. We use ReLU activation in the hidden layers and tanh activation at the output layer.

2) *Reward Functions*: The reward function is used to shape the actions of the end-to-end DRL network, i.e., to encourage (through positive rewards) desirable and discourage (through negative rewards) undesirable robot velocities. This in turn trains the intermediate feature vectors (such as F_{ref}) in the DRL network to learn features that are relevant for safe robot navigation (leading to high rewards). The total reward collected by the robot for performing an action at any instant is given as,

$$R_{tot} = \beta_1 R_{dist} + \beta_2 R_{head} + \beta_3 R_{stable} + \beta_4 R_{grad}. \quad (4)$$

Here, the different β are the weighing factors for the different reward components. R_{dist} and R_{head} , are the penalties for the robot moving away from its goal. They are defined as,

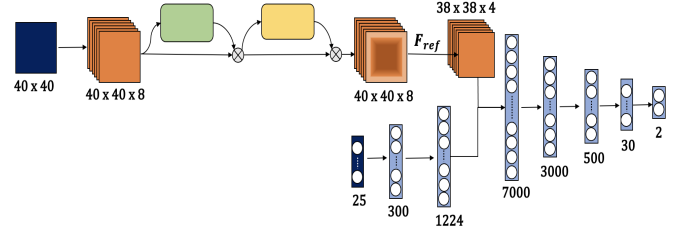


Fig. 3: The network architecture of our DRL network. The dark blue layers represent our normalized elevation map and the vector containing the robot's pose, goal, and elevation gradient-related vectors. The orange layers represent convolutional layers, and the light blue layers represent fully connected layers. The green and yellow blocks represent the channel and spatial attention modules, respectively. The dimensions of each layer are mentioned beside it. Our network is computationally light enough to run in real-time on a laptop GPU.

$$R_{dist} = -d_{goal}, \quad R_{head} = -|\alpha_{goal}|. \quad (5)$$

R_{stable} is the reward for the robot maintaining stability (having low roll and pitch angles) and is defined as,

$$R_{stable} = \cos^2 \phi + \cos^2 \theta. \quad (6)$$

R_{head} is the penalty for heading in a direction with a high elevation gradient. It is defined as,

$$R_{head} = -\mathbf{w} \cdot \mathbf{g}, \quad (7)$$

where \mathbf{w} is a weight vector with weights in the ascending order, and \mathbf{w} is the heading gradient vector defined in Equation 2. The \mathbf{w} vector weighs elevation changes that are closer to the robot higher than the ones farther away.

3) *Attention Mask Extraction*: As mentioned in Section III-B, we extract a spatial attention map A from the refined feature vector F_{ref} . Since F_{ref} 's different channels are already weighted by the channel and spatial attention modules, the attention mask can be obtained by an unweighted summation along the channels. This is,

$$A(i, j) = \sum_{i=1}^8 F_{ref}(x, y, i). \quad (8)$$

The attention mask highlights decreased stability locations that are relevant for the robot's motion. For instance, say the robot is turning to the right. The attention mask weighs elevation changes in that direction higher than all other directions. For example, Fig.4(b) depicts the attention mask corresponding to the input elevation map presented in Fig.4(a), where the robot is attempting to make a right turn. The attention mask weights are biased towards the critical elevation gradients on the right side of the robot.

C. Computing Navigation Cost-map

Since the normalized elevation map and the attention mask represent the environment's elevation values and the weights for the different regions, we utilize them to compute a navigation cost-map as,

$$C(i, j) = E_N(i, j) \odot A(i, j). \quad (9)$$

Here \odot represents element-wise multiplication. The computed costmap is shown in Fig.4(c). To completely avoid certain high-cost regions (costs higher than a certain threshold C_{max}) while navigating, we perform the following operation.

$$C(i, j) = \infty \quad \text{if} \quad C(i, j) > C_{max}. \quad (10)$$

D. Computing Least-cost Waypoints

Consider a local cost-map $C(i, j)$ and a goal location \mathbf{g} that lies outside it. Choosing least-cost waypoints (some location (i, j)) inside $C(i, j)$ that lead the robot towards its goal is non-trivial. This is because the robot operates without any global knowledge of the environment. In addition, the chosen waypoint must be safely reachable by the robot. To address this, we formulate the following method.

Given a robot with its goal at \mathbf{g} , we consider an approximate circle $\mathcal{C}_{explore}$ in $C(i, j)$ centered at the robot with a radius $r_{explore} < r_{sense}$. Next, we consider an arc \mathcal{A}_1 on the circumference of $\mathcal{C}_{explore}$ that makes an angle of $\gamma_{explore}$ at the center with the goal vector \mathbf{g} bisecting it (see Fig.4(d)). We use all locations $(i, j) \in \mathcal{A}_1$ as candidate waypoints. We then choose the *least-cost* waypoint locations in the cost-map as,

$$L_{min} = \{\operatorname{argmin}_{(i, j) \in \mathcal{A}_1} (\operatorname{cost}((i, j)))\}. \quad (11)$$

Here, for $\operatorname{cost}((i, j))$ is the cumulative cost of navigating to (i, j) from the robot's location $(0, 0)$ in the cost-map by trajectories computed by Dijkstra's algorithm [32]. If multiple index locations exist in L_{min} , we choose the waypoint by transforming it to real-world coordinates (see Equation 1) as,

$$x^*, y^* = \operatorname{argmin}_{x, y \in (res \cdot L_{min})} (\operatorname{dist}((x, y), \mathbf{g})). \quad (12)$$

In the highly unlikely event that $L_{min} = \emptyset$ (implying all trajectories have infinite cost), we expand the arc \mathcal{A}_1 to \mathcal{A}_2 , which makes an angle of $2 \cdot \gamma_{explore}$ at $\mathcal{C}_{explore}$'s center. We then consider $(i, j) \in \mathcal{A}_2 \setminus \mathcal{A}_1$ as candidate waypoints and repeat the procedure.

When the terrain is planar, the robot can safely have a larger exploration circle and choose waypoints on its circumference. This would significantly reduce the number of waypoints that need to be computed before reaching the goal. Therefore, $r_{explore}$ is formulated as a function of the costs within the circle as,

$$r_{explore} = k_1 + k_2 \cdot \frac{1}{\operatorname{mean}(C(i, j))}; \quad \forall i, j \in \mathcal{C}_{explore}. \quad (13)$$

where k_1 and k_2 are constants. If the costs within $\mathcal{C}_{explore}$ are low (implying a planar surface), the formulation expands the radius.

Proposition IV.1. *Our method always navigates the robot in the safest possible path locally such that the robot does not flip over.*

Proof. This result follows from the fact that the waypoints computed using Equation 12 are reachable with the least trajectory cost locally. In addition, since our cost-map has infinite costs for unsafe regions, such regions are guaranteed to be avoided when selecting waypoints. ■

E. Integration with DWA-RL

We use DWA-RL [8] to compute robot velocities to follow the least-cost trajectory computed by Dijkstra's algorithm. DWA-RL guarantees that the velocities are collision-free and are dynamically feasible/achievable for the robot. Therefore, the robot can avoid collisions with dynamic obstacles in the environment.

Fig. 2 shows how the components in our method are connected. Our approach decouples perception to our DRL network with the attention modules and the navigation to our local waypoint computation and DWA-RL. This architecture drastically improves the sim-to-real transfer capabilities and allows for guarantees on the waypoint costs and the dynamic feasibility of the final velocities.

REFERENCES

- [1] A. Bonci, P. D. Cen Cheng, M. Indri, G. Nabissi, and F. Sibona, "Human-robot perception in industrial environments: A survey," *Sensors*, vol. 21, no. 5, p. 1571, 2021.
- [2] F. Vulpi, A. Milella, R. Marani, and G. Reina, "Recurrent and convolutional neural networks for deep terrain classification by autonomous robots," *Journal of Terramechanics*, 2021.
- [3] E. Kayacan and G. Chowdhary, "Tracking error learning control for precise mobile robot path tracking in outdoor environment," *Journal of Intelligent & Robotic Systems*, vol. 95, no. 3, pp. 975–986, 2019.
- [4] K. Zakharov, A. Saveliev, and O. Sivchenko, "Energy-efficient path planning algorithm on three-dimensional large-scale terrain maps for mobile robots," in *International Conference on Interactive Collaborative Robotics*. Springer, 2020, pp. 319–330.
- [5] A. H. Qureshi, A. Simeonov, M. J. Bency, and M. C. Yip, "Motion planning networks," in *2019 International Conference on Robotics and Automation (ICRA)*. IEEE, 2019, pp. 2118–2124.
- [6] H. Hu, K. Zhang, A. H. Tan, M. Ruan, C. Agia, and G. Nejat, "A sim-to-real pipeline for deep reinforcement learning for autonomous robot navigation in cluttered rough terrain," *IEEE Robotics and Automation Letters*, vol. 6, no. 4, pp. 6569–6576, 2021.
- [7] N. Ganganath, C.-T. Cheng, and K. T. Chi, "A constraint-aware heuristic path planner for finding energy-efficient paths on uneven terrains," *IEEE transactions on industrial informatics*, vol. 11, no. 3, pp. 601–611, 2015.
- [8] U. Patel, N. Kumar, A. J. Sathiyamoorthy, and D. Manocha, "Dynamically feasible deep reinforcement learning policy for robot navigation in dense mobile crowds," 2020.
- [9] S. Woo, J. Park, J.-Y. Lee, and I. S. Kweon, "Cbam: Convolutional block attention module," in *Proceedings of the European Conference on Computer Vision (ECCV)*, September 2018.
- [10] D. Kim, J. Sun, S. M. Oh, J. M. Rehg, and A. F. Bobick, "Traversability classification using unsupervised on-line visual learning for outdoor robot navigation," in *Proceedings 2006 IEEE International Conference on Robotics and Automation, 2006. ICRA 2006*. IEEE, 2006, pp. 518–525.
- [11] B. Liu, M. Adams, and J. Ibanez-Guzman, "Multi-aided inertial navigation for ground vehicles in outdoor uneven environments," in *Proceedings of the 2005 IEEE International Conference on Robotics and Automation*. IEEE, 2005, pp. 4703–4708.
- [12] L. Nardi and C. Stachniss, "Actively improving robot navigation on different terrains using gaussian process mixture models," in *2019 International Conference on Robotics and Automation (ICRA)*. IEEE, 2019, pp. 4104–4110.
- [13] K. M. Wurm, R. Kümmerle, C. Stachniss, and W. Burgard, "Improving robot navigation in structured outdoor environments by identifying vegetation from laser data," in *2009 IEEE/RSJ International Conference on Intelligent Robots and Systems*. IEEE, 2009, pp. 1217–1222.
- [14] C. Wellington, A. Courville, and A. Stentz, "A generative model of terrain for autonomous navigation in vegetation," *The International Journal of Robotics Research*, vol. 25, no. 12, pp. 1287–1304, 2006.
- [15] C. Bai, J. Guo, and H. Zheng, "Three-dimensional vibration-based terrain classification for mobile robots," *IEEE Access*, vol. 7, pp. 63 485–63 492, 2019.
- [16] J. Zürn, W. Burgard, and A. Valada, "Self-supervised visual terrain classification from unsupervised acoustic feature learning," *IEEE Transactions on Robotics*, vol. 37, no. 2, pp. 466–481, 2021.

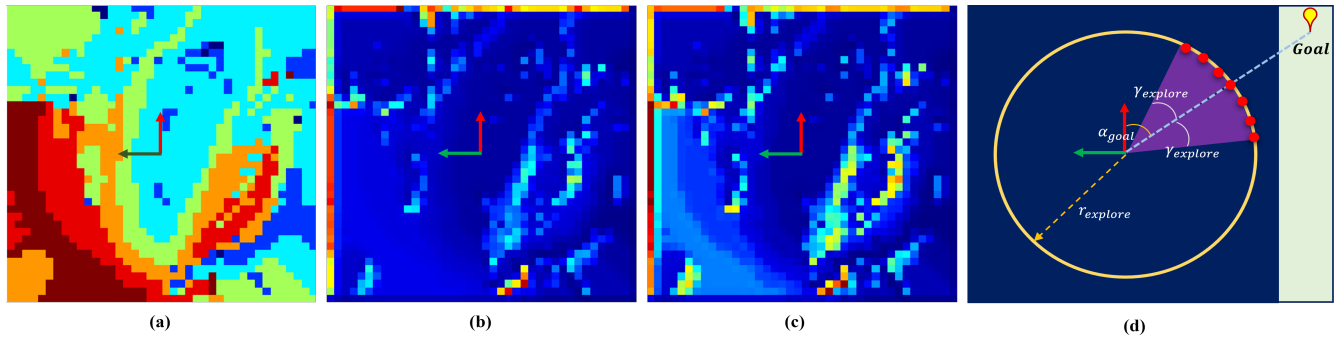


Fig. 4: Computing navigation cost-map and waypoints: (a) Input elevation map; (b) Attention mask; (c) Cost-map; (d) Least cost waypoint computation

- [17] W. Wang, B. Zhang, K. Wu, S. A. Chepinskiy, A. A. Zhilenkov, S. Chernyi, and A. Y. Krasnov, "A visual terrain classification method for mobile robots' navigation based on convolutional neural network and support vector machine," *Transactions of the Institute of Measurement and Control*, p. 0142331220987917, 2021.
- [18] A. Hornung, K. M. Wurm, M. Bennewitz, C. Stachniss, and W. Burgard, "OctoMap: An efficient probabilistic 3D mapping framework based on octrees," *Autonomous Robots*, 2013, software available at <http://octomap.github.com>. [Online]. Available: <http://octomap.github.com>
- [19] P. Fankhauser, M. Bloesch, C. Gehring, M. Hutter, and R. Siegwart, "Robot-centric elevation mapping with uncertainty estimates," in *International Conference on Climbing and Walking Robots (CLAWAR)*, 2014.
- [20] P. Fankhauser, M. Bloesch, and M. Hutter, "Probabilistic terrain mapping for mobile robots with uncertain localization," *IEEE Robotics and Automation Letters (RA-L)*, vol. 3, no. 4, pp. 3019–3026, 2018.
- [21] D. C. Guastella and G. Muscato, "Learning-based methods of perception and navigation for ground vehicles in unstructured environments: a review," *Sensors*, vol. 21, no. 1, p. 73, 2021.
- [22] S. Laubach, J. Burdick, and L. Matthies, "An autonomous path planner implemented on the rocky 7 prototype microrover," in *Proceedings. 1998 IEEE International Conference on Robotics and Automation (Cat. No.98CH36146)*, vol. 1, 1998, pp. 292–297 vol.1.
- [23] M. Pivtoraiko, R. A. Knepper, and A. Kelly, "Differentially constrained mobile robot motion planning in state lattices," *Journal of Field Robotics*, vol. 26, no. 3, pp. 308–333, 2009.
- [24] S. Shimoda, Y. Kuroda, and K. Iagnemma, "Potential field navigation of high speed unmanned ground vehicles on uneven terrain," in *Proceedings of the 2005 IEEE International Conference on Robotics and Automation*, 2005, pp. 2828–2833.
- [25] F. G. Oliveira, A. A. Neto, D. Howard, P. Borges, M. F. Campos, and D. G. Macharet, "Three-dimensional mapping with augmented navigation cost through deep learning," *Journal of Intelligent & Robotic Systems*, vol. 101, no. 3, pp. 1–21, 2021.
- [26] D. Silver, J. A. Bagnell, and A. Stentz, "Learning from demonstration for autonomous navigation in complex unstructured terrain," *The International Journal of Robotics Research*, vol. 29, no. 12, pp. 1565–1592, 2010.
- [27] R. Valencia-Murillo, N. Arana-Daniel, C. López-Franco, and A. Y. Alanís, "Rough terrain perception through geometric entities for robot navigation," in *2nd International Conference on Advances in Computer Science and Engineering (CSE 2013)*. Atlantis Press, 2013, pp. 1–2.
- [28] K. Zhang, F. Niroui, M. Ficocelli, and G. Nejat, "Robot navigation of environments with unknown rough terrain using deep reinforcement learning," in *2018 IEEE International Symposium on Safety, Security, and Rescue Robotics (SSRR)*. IEEE, 2018, pp. 1–7.
- [29] A. Nguyen, N. Nguyen, K. Tran, E. Tjiputra, and Q. D. Tran, "Autonomous navigation in complex environments with deep multi-modal fusion network," in *2020 IEEE/RSJ International Conference on Intelligent Robots and Systems (IROS)*, 2020, pp. 5824–5830.
- [30] S. Josef and A. Degani, "Deep reinforcement learning for safe local planning of a ground vehicle in unknown rough terrain," *IEEE Robotics and Automation Letters*, vol. 5, no. 4, pp. 6748–6755, 2020.
- [31] T. P. Lillicrap, J. J. Hunt, A. Pritzel, N. Heess, T. Erez, Y. Tassa, D. Silver, and D. Wierstra, "Continuous control with deep reinforcement learning," 2019.
- [32] J.-C. Chen, "Dijkstra's shortest path algorithm," *Journal of formalized mathematics*, vol. 15, no. 9, pp. 237–247, 2003.